https://doi.org/10.5564/mgs.v30i61.3957

Mongolian Geoscientist

Original Article

Monitoring Vegetative Stages of Spring Wheat (*Triticum Aestivum* L) with Sentinel-1 and Sentiel-2 Imagery in Bornuur soum, Tuv province, Mongolia

Sanjaatjamts Lkhagvadulam[1], Gansukh Badamgarav[2], Batsaikhan Bayartungalag[3], Dursahinhan Tsogtsaikhan Altangerel[4], Bold Odgerel[1*]

[1]*Disaster Studies Center, Research Institute, University of Internal Affairs, Ulaanbaatar 13260, Mongolia*
[2]*School of Agroecology, University of Life Sciences, Ulaanbaatar 17024, Mongolia*
[3]*Institute of Geography and Geoecology, Mongolian Academy of Sciences, Ulaanbaatar 15170, Mongolia*
[4]*Harold W. Manter Laboratory of Parasitology, University of Nebraska-State Museum, University of Nebraska-Lincoln, Lincoln Nebraska 68588, USA*

**Corresponding author:odgerel.b@uia.gov.mn, ORCID: 0000-0003-2575-8662*

ARTICLE INFO

Article history:

Received: 11 March, 2025
Revised: 23 September, 2025
Accepted: 28 September, 2025

ABSTRACT

Spring wheat (*Triticum aestivum* Linnaeus, 1753) is critical for global food security, sustaining over 20% of the world's population. In Mongolia, it is the primary staple crop, though production is affected by climatic and market fluctuations. This study, conducted at the "Nart" Research Center of the Mongolian University of Life Sciences in Bornuur soum, Tuv province, examined growth dynamics of the Darkhan-144 wheat variety using Sentinel-1 and Sentinel-2 satellite data. The crop, sown between May 21-25, 2020, achieved uniform germination within 15-20 days. Key phenophases included germination to main pricking (10 days), heading (15 days), flowering to milky seed stage (15 days), and milky to hybrid tuber (10 days), totaling a growth cycle of 85-90 days. The Normalized Difference Vegetation Index rose from (~0.18) in early May to 0.80 by July and September. Normalized Difference Vegetation Index showed strong correlation with the Normalized Difference Water Index for wet biomass (R^2=0.67) and dry biomass (R^2=0.62). Sentinel-2 reflectance ranged from 0.05-0.40 in May and July, and 0.25-0.45 in June. Field spectrometer values increased from 0.35 in July to 0.60 nm in August, before declining to 0.30 nm in September. These findings reveal a strong correlation between vegetation water indices and wheat growth parameters, highlighting the potential of satellite-based spatiotemporal analysis to inform and enhance local policymaking in agricultural production and management. This study supports the integration of remote sensing into Mongolia's crop monitoring strategies.

Keywords: NDVI analysis, crop phenology, biomass estimation, remote sensing agriculture, vegetation indices, spatiotemporal monitoring

INTRODUCTION

Climate extremes, such as drought and heat-waves, often affect major breadbaskets simultaneously, posing significant threats to global food security (Kornhuber et al., 2019). Wheat, believed to have evolved from wild grass and first cultivated between 15,000 and 10,000 BC, is an annual plant of the genus Triticum, which includes common bread wheat (*Triticum aestivum*) and durum wheat (T*riticum turgidum*) (Shewry, 2009).

In Mongolia, wheat remains a staple crop, yet farmers frequently face challenges due to the lack of satellite-based data for accurately estimating crop vegetation and growth dynamics (Gansukh et al., 2020; Tuvdendorj et al., 2019). Despite its importance, Mongolian wheat farmers face challenges due to the lack of

satellite-based data for accurately estimating crop vegetation. Monitoring wheat yields at both regional and national levels is critical for agricultural policy, food security, and economic management, especially given the increasing impacts of climate change (Toth and Jóźków, 2016; Trivellone et al., 2022). Regional climate changes, such as reduced precipitation and rising temperatures, threaten crop yields, emphasizing the urgency of studies that improve monitoring and management systems (IPCC, 2021; Zhao et al., 2020).

Climate change intensifies these risks by disrupting pathogen-host relationships and promoting the geographic expansion of both pathogens and their hosts (Brooks et al., 2019; Brooks and Agosta, 2024a). Increased temperatures, altered precipitation patterns, and higher atmospheric CO_2 levels create ideal conditions for the proliferation of both existing and emerging pathogens, allowing them to spread into new regions (Zhao et al., 2020). For wheat crops, this results in greater vulnerability to fungal infections, rust diseases, and bacterial blights (Brooks et al., 2019). Furthermore, environmental changes drive pathogen host shifts, introducing new diseases that local wheat varieties are often ill-equipped to withstand, jeopardizing yield stability (IPCC, 2021).

Globally, various techniques have been adopted for early estimation of crop yields, categorized into field surveys, remote sensing (RS) methods, and crop modeling, often used in combination. Field surveys, for example, use random sampling techniques to develop regional and national forecasts, as demonstrated by initiatives like Harvest Choice. In North China, MODIS data has been used to adjust the WOFOST model for wheat growth monitoring, improving crop model performance at regional scales (Yuping et al., 2008). Remote sensing approaches have advanced rapidly, with novel frameworks fusing Sentinel-1 SAR, Sentinel-2 optical data, and high-resolution climate information. For instance, recent studies have shown that integrating Sentinel-1 and Sentinel-2 datasets significantly improves the classification and monitoring accuracy of cereal crops such as barley and wheat (Ibrahim et al., 2023). Similarly, research in Germany demonstrated that combining radar, optical, and climate data through a machine learning framework enhances the accuracy of crop phenology detection across multiple crops and growth stages (Shojaeezadeh et al., 2025). Additionally, Sentinel-2 derived vegetation indices, such as NDVI and NDWI, have proven effective in estimating within-field wheat grain yield under heterogeneous field conditions (Segarra et al., 2022). These advances, combined with local studies on crop stress monitoring using Landsat-8 imagery, underscore the importance of satellite-based spatiotemporal analysis for wheat management in Mongolia (Tuvshinbayar et al., 2018). Integrating high-resolution satellite imagery, vegetation indices, and climate data provides essential insights for improving wheat monitoring and management, supporting timely agricultural decision-making, and mitigating risks from climate variability and emerging agricultural threats.

This study focuses on monitoring the lifecycle and growth of common wheat (*Triticum aestivum* L.) in Mongolia using integrated remote sensing techniques. Specifically, we aim to: (1) determine phenological stages of wheat through field measurements; (2) assess growth and moisture content using Normalized Difference Vegetation Index (NDVI) and Normalized Difference Water Index (NDWI) derived from Sentinel-2 satellite data; and (3) monitor vegetation and water content through VV and VH polarization data from Sentinel-1 SAR imagery. These efforts provide critical insights for improving wheat management strategies in Mongolia's increasingly volatile climate.

MATERIALS AND METHOD

Study Area

This study was conducted in a wheat-dominated agricultural region in Bornuur soum, Tuv province, Mongolia (Fig. 1), located between 48°16'53"N-48°41'26"N and 105°59'11"E-106°32'05"E. The primary crop in this area is wheat (*Triticum aestivum* L.). The phenological stages of wheat cultivation in this region include the heading stage from early June to late August, the grain-filling stage before late August, and milk maturity in mid-July. Wheat

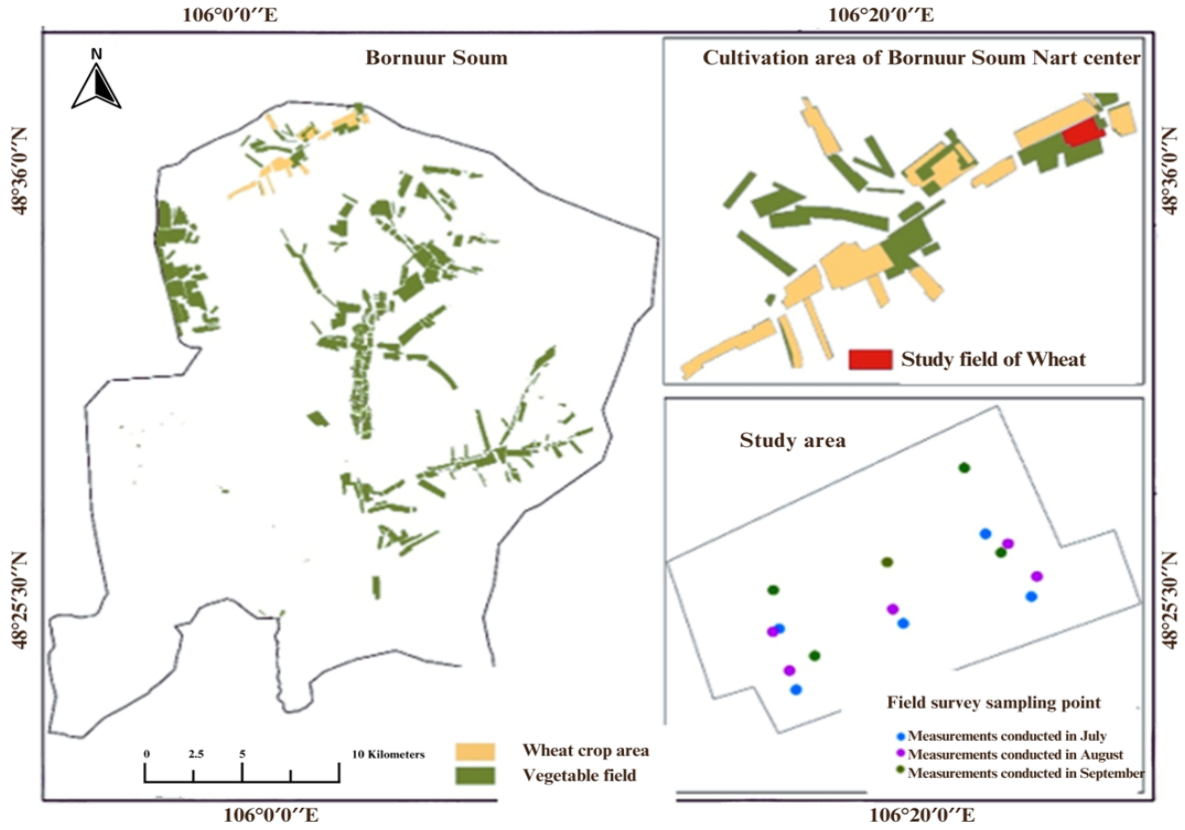

Fig. 1. Location of study area and visualization of agricultural areas

is typically sown in May and harvested in September, aligning with the spring growing season. Tuv province is Mongolia's principal grain-producing region, contributing over 45% of the nation's total wheat production. Most of the cultivated land in this area is rain-fed cropland, making wheat yields highly dependent on weather conditions. The region averages between 90 to 110 frost-free days and has annual mean precipitation between 250 and 400 mm. In addition, crop growing duration is short (90-140 days) in this region, depending on location and altitude. Approximately 90% of the nationwide precipitation is lost to evapotranspiration, which is associated with a continental climate. The region is also characterized by several distinct soil types, which play a crucial role in agricultural productivity (Tuvdendorj et al., 2019). These environmental and climatic conditions emphasize the importance of monitoring and managing key factors to optimize wheat yields in Tuv province. Bornuur soum experiences relatively low rainfall, warm summers, and low humidity, which further challenge wheat cultivation.

DATA AND PROCESSING

Yield Data

The wheat yield data for this study was obtained from the "Nart" Research Center of the Mongolian University of Life Sciences, located in Bornuur soum, Tuv province, Mongolia. Data collection involved determining the phenological stages of the plant through field measurements, utilizing field survey-based approaches with random sampling techniques practiced in the wheat fields. After planting, 20 consecutive wheat plants were observed every five days from the center of the field until 70% of the plants reached the dough development stage. Key observations and recordings included estimated plant pods at this critical growth phase.

The study aimed at:

1. Determine the phenological stages of spring wheat (*Triticum aestivum* L.) through systematic field measurements.
2. Assess the growth and moisture content of spring wheat cultivation in the study area using the Normalized Vegetation Index (NDVI) and Normalized Difference Water Index (NDWI) values. These indices were

developed from multi-channel spectral data obtained from the European Space Agency's Sentinel-2 satellite, providing crucial insights into crop health and moisture status.

This integrated approach combining ground-based observations and satellite remote sensing offers a comprehensive framework for monitoring wheat growth and optimizing yield estimation in the region.

Satellite Data

Both optical and radar remote sensing data used in this study were derived from Sentinel-2 MSI and Sentinel-1 SAR datasets (Table 1). A total of 22 time-series Sentinel-1A images were utilized, with Ground Range Detected (GRD) data that were preprocessed, including focusing, multilooking, calibration, and ground-range projection. The data were terrain-corrected, normalized, and calibrated using local incidence angles and cosine correction before being converted to sigma naught (σo dB) for mapping and analysis. All Sentinel satellite images were freely downloaded from the Sentinel Hub, developed by the European Space Agency (ESA) https://www.sentinel-hub.com/

Key indices were employed for monitoring wheat growth:

1. NDVI is defined as the ratio of the difference between the near-infrared band (NIR) and the visible red band (RED) to their sum. It can be expressed using Equation (1) (Shao et al., 2016) and was derived from Sentinel-2 data.

Table 1. Dates of Sentinel-1 and Sentinel-2 data acquisition for the study area

Sentinel-1/Date (calibration, terrain- correction)	Sentinel-2/Date
3 May 2020	7 May 2020
10 May 2020	27 May 2020
27 May 2020	26 Jun 2020
3 Jun 2020	6 Jul 2020
15 Jun 2020	21 Jul 2020
27 Jun 2020	31 Jul 2020
9 Jul 2020	
14 Jul 2020	
26 Jul 2020	
2 Aug 2020	4 Sep 2020
14 Aug 2020	19 Sep 2020
26 Aug 2020	
7 Sep 2020	
19 Sep 2020	

2. NDWI (Equation 2; Gao, 1996) is calculated using Sentinel-2 bands 8A (865 nm) and 11 (1610 nm). This index is valuable for assessing vegetation water content across large areas and supports decision-making for harvest management.

Additionally, monitoring was conducted based on the VV and VH polarizations of Sentinel-1 SAR data. These polarizations were used to calculate changes in common wheat (*Triticum aestivum* L.) vegetation and the water content of plant leaves, providing critical insights into crop health and growth dynamics.

$$NDVI=(Band8-Band4)/(Band8+Band4) \quad (1)$$

$$NDWI=(Band8A-Band11)/(Band8A+Band11) \quad (2)$$

Crop Height Monitoring and Methodology

Crop height was assessed across different development stages using machine-learning algorithms, including Random Forest Regression (RFR), Support Vector Machine Regression (SVMR), Neural Network Regression (NNR), and Decision Tree Regression (DTR). Sentinel-1 SAR imagery underwent preprocessing steps such as terrain correction, radiometric calibration, and despeckling, while Sentinel-2 optical imagery was atmospherically corrected, resampled, and converted into spectral indices relevant for vegetation monitoring. Time-series datasets spanning multiple months were used to capture the phenological dynamics of wheat growth, allowing for more accurate modeling of crop height variability. The machine-learning algorithms were first applied independently to Sentinel-1 SAR data and subsequently to fused datasets combining SAR and optical information. Data fusion incorporated polarization backscatter indices from Sentinel-1 and spectral vegetation indices from Sentinel-2, enhancing model input features. Hyperparameter tuning and cross-validation procedures were employed to optimize algorithm performance. Model accuracy was evaluated using coefficient of determination (R^2) and root mean square error (RMSE), and the contribution of individual predictor variables was analyzed to identify key factors influencing wheat crop height (Nduku et al., 2024). This integrated approach

provides a robust framework for monitoring wheat biophysical parameters and can support decision-making in agricultural management.

RESULTS

Uniformity of growth and development stages of wheat plants

The growth and development stages of wheat plants were closely monitored from sowing until the plants reached the uniform pod stage, which was defined as 70% of the estimated plants bearing pods. Observations were conducted every five days on 20 consecutive plants at a pre-selected point in the central part of the wheat field. The dates and stages of plant growth were carefully recorded to establish a detailed timeline of development. Sowing was conducted during the second ten-day period of May 2020. Germination began in the first ten days of June and became uniform by the second ten days of June. By the last ten days of June, the plants had reached a uniform protrusion stage, characterized by the initial emergence of shoots. The germination and early seedling establishment were consistent with the images of the Germination Stage (Fig. 2a) and Seedling Stage (Fig. 2b), with plant growth becoming visibly uniform by the second half of June. During the second ten days of July, the plants entered the main heading stage. This phase progressed steadily through the final ten days of July. The main heading stage, or Tillering and Elongation Stages, is depicted in (Fig. 2c and 2d) These stages are crucial for the plant's early vertical growth and the development of its branches. During this period, the wheat plants began forming a distinct heading structure, which is represented in (Fig. 2e). Uniform flowering, which marked the Anthesis Stage, occurred in the second ten days of August, as the wheat plants began to produce flowers simultaneously. This flowering stage is clearly visualized in (Fig. 2f), highlighting the uniformity and synchronization of the flowering process. By the last ten days of August, the plants entered the milk stage. This milk maturity phase is typically characterized by the development of a milky liquid inside the grains, as shown in (Fig. 2g) Grain filling was completed by the first ten days of September, signaling the completion of the Grain Filling Stage (Fig. 2h). During this phase, the plant focuses on filling the kernels with starch and nutrients, finalizing the crop's growth cycle before harvest. The wheat yields stabilized during this period, and harvesting was completed during the second ten days of September. In this region, the phenological stages of wheat are divided into several key phases: the heading stage, which occurs from early June to late August, the grain-filling stage, which happens before late August, and the milk maturity stage in mid-July. These stages are consistent with the typical growing pattern in Mongolia, where wheat is planted in May during the spring growing season and matures by September. This timeline highlights the critical stages of wheat growth and the environmental conditions essential for successful wheat cultivation in this area.

Result of Sentinel-2 satellite, determination of crop moisture content

The correlation between the moisture index (NDWI) and the wet weight biomass of common wheat (*Triticum aestivum* L.) was found to be strong, with a numerical value of R^2=0.67.

Fig. 2. NDVI-based vegetation condition of Bornuur soum showing the degraded areas in the southwest section during the 2020 drought season

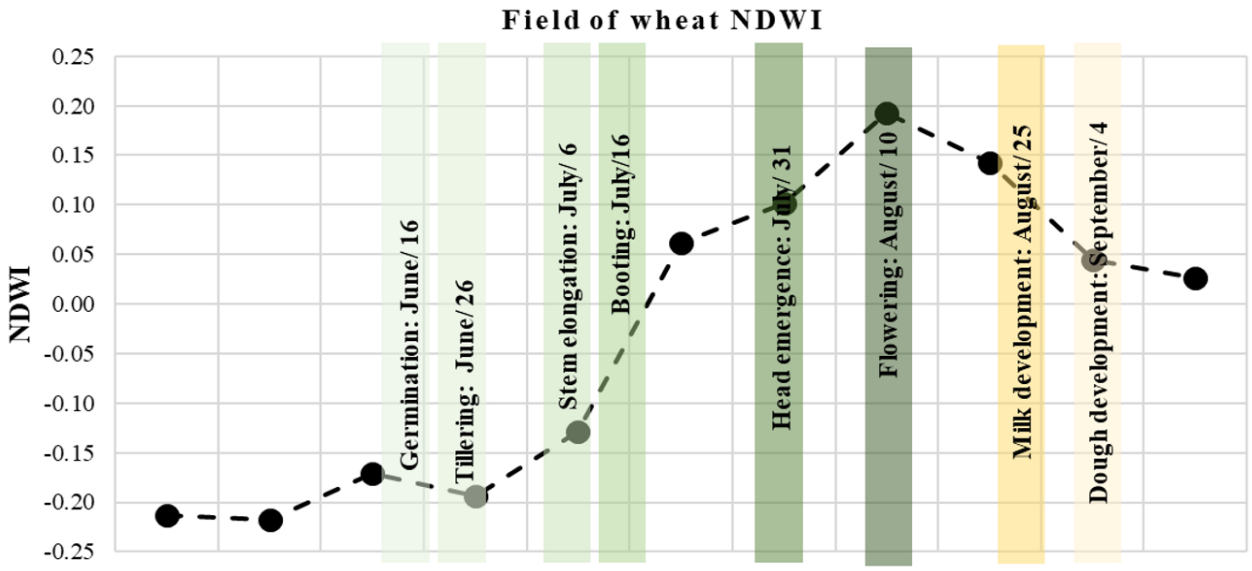

Fig. 3. Spatial distribution of NDWI in using Sentinel-2 with the wheat growing season of 2020

Additionally, wheat is highly sensitive to waterlogging, which reduces soil oxygen levels, thereby impairing root function and survival.

As shown in (Fig. 3), the Normalized Difference Water Index (NDWI) values for wheat plants were tracked across various phenological stages, highlighting changes in water content throughout the growing season. The graph demonstrates that during the germination phase (June 16), the NDWI values were low, reflecting the initial growth stage where water retention is minimal. As the wheat plants progressed into the tillering and stem elongation stages (June 26 to July 6), there was a gradual increase in NDWI, indicating an increase in water absorption as the plants became more established. During the booting phase (July 16), the NDWI continued to rise, reaching a peak as the wheat plants entered the heading and flowering stages (July 31 to August 10). The NDWI values remained high during the reproductive stages, showing that the plants were actively utilizing water for reproductive growth. By the time the plants reached the milk development (August 25) and dough development (September 4) stages, NDWI began to decrease, reflecting the plant's transition from vegetative and reproductive growth to grain maturation, with less water absorbed as the grains filled and matured.

The graph in (Fig. 4) shows the relationship between the Normalized Difference Water Index (NDWI) and the wet weight biomass of common wheat. The x-axis represents the wet weight biomass of the wheat plants (measured in grams), while the y-axis represents the NDWI values, which indicate the water content in the plants. The data points show a positive correlation between the wet weight biomass and NDWI, suggesting that as the wet weight of the wheat biomass increases, so does the water content (measured by NDWI). This is expected, as larger, more mature plants tend to have higher water content. The R^2 value of 0.67 indicates a moderate correlation between the two variables, meaning that approximately 67% of the variation in NDWI can be explained by the wet weight biomass of the wheat plants. Although the relationship is positive, the moderate R^2 suggests that other factors may also influence the NDWI values.

Fig. 5 shows the NDVI values for the crop area between May and September 2020. The NDVI value for common wheat in the study

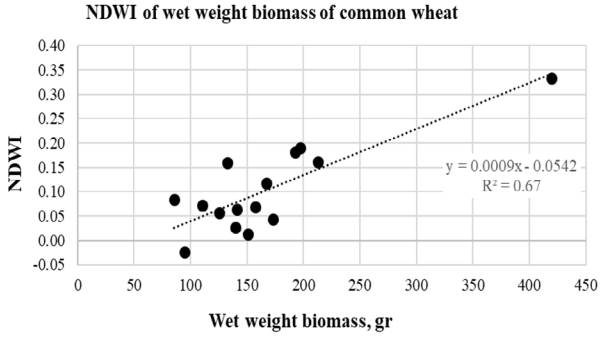

Fig. 4. Wet weight biomass, gr

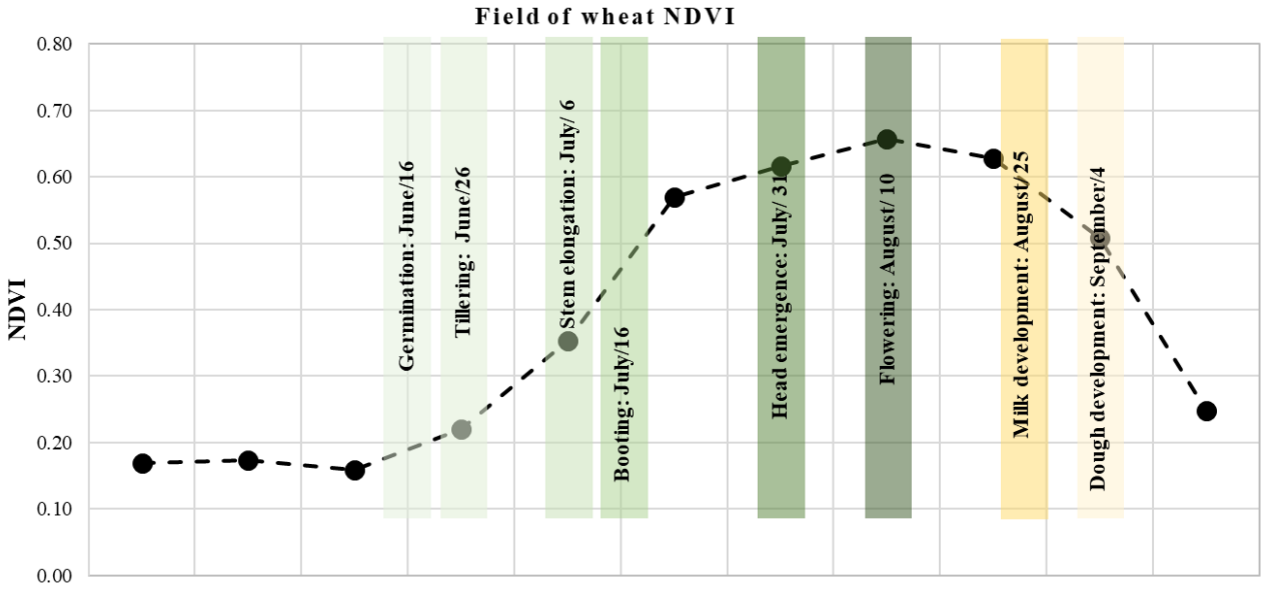

Fig. 5. Field of wheat NDVI compared to the value of NDVI of dry weight

area was initially low in early May (~0.18), reflecting minimal vegetation or plant cover at the beginning of the growing season. However, the NDVI increased significantly over the following months, reaching a peak of around 0.8 in July and remaining high through September, indicating healthy, dense vegetation and active growth during the peak growing season.

Fig. 6 shows the relationship between NDVI and dry weight biomass of common wheat. As the dry weight biomass increases, the NDVI values also increase, indicating better plant health and higher vegetation density. The R^2 value of 0.62 suggests a moderate correlation between the two variables, meaning that 62% of the variation in NDVI can be explained by changes in dry weight biomass. This indicates that while NDVI is a useful indicator of biomass, other factors may also influence its values.

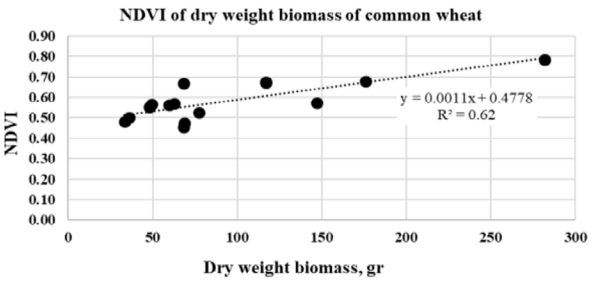

Fig. 6. Dry weight biomass, gr

Spectral measurements of wheat cultivation

Sentinel-2 satellite measurements from May to September 2020 showed that the reflectance values ranged from 0.05 to 0.20 nm in the first ten days of the five months, and 0.35 to 0.40 nm in the last ten days of the month. In June, the wavelength was 0.25-0.35 nm in the first ten days, and 0.40-0.45 nm in the last ten days of the month. In the first ten days of July, the wavelength was 0.05-0.25 nm, and in the last ten days, the wavelength was 0.30-0.40 nm, while the field measurement results were 0.35 nm. Sentinel-2 satellite measurements from May to September 2020 showed that the reflectance values ranged from 0.05 to 0.20 nm in the first ten days of the five months, and 0.35 to 0.40 nm in the last ten days of the month. In June, the wavelength was 0.25-0.35 nm in the first ten days, and 0.40-0.45 nm in the last ten days of the month. In the first ten days of July, the wavelength was 0.05-0.25 nm, and in the last ten days, the wavelength was 0.30-0.40 nm, while the field measurement results were 0.35 nm.

Fig. 7 shows the changes in Sentinel-2 wavelengths for a wheat field in Nart over the months of June, July, August, and September 2020. The x-axis represents the wavelength range from 350 to 2350 nm, while the y-axis indicates the wavelength values corresponding to different growth stages of the wheat plants. The graph displays several distinct stages of growth: Leaf Pigment (Green range): The wavelengths related to leaf pigments increase during flowering (green line), suggesting

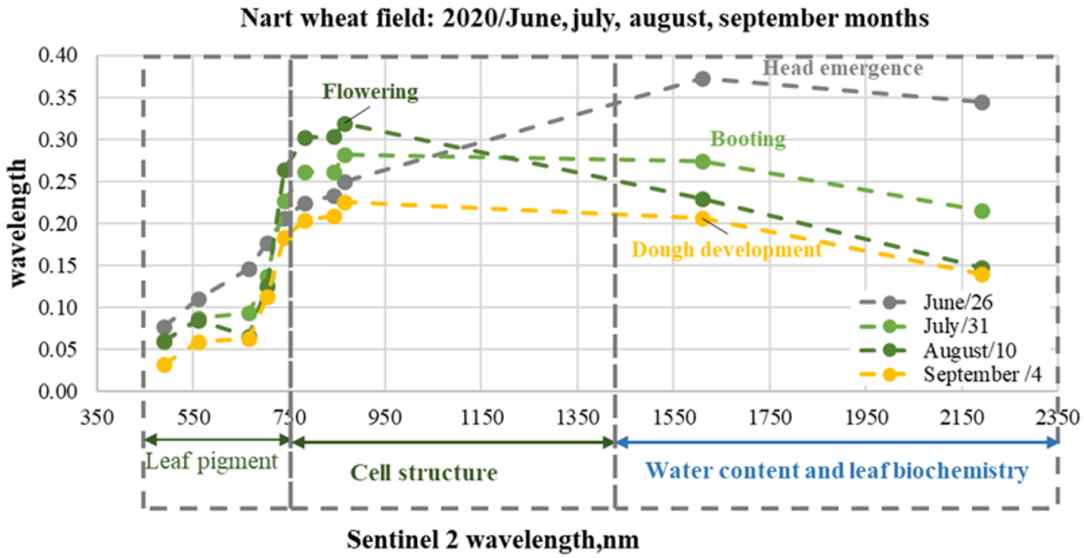

Fig. 7. Results of Sentinel satellite calculations and field measurements of Nart Field, wavelength of Sentinel-2, nm

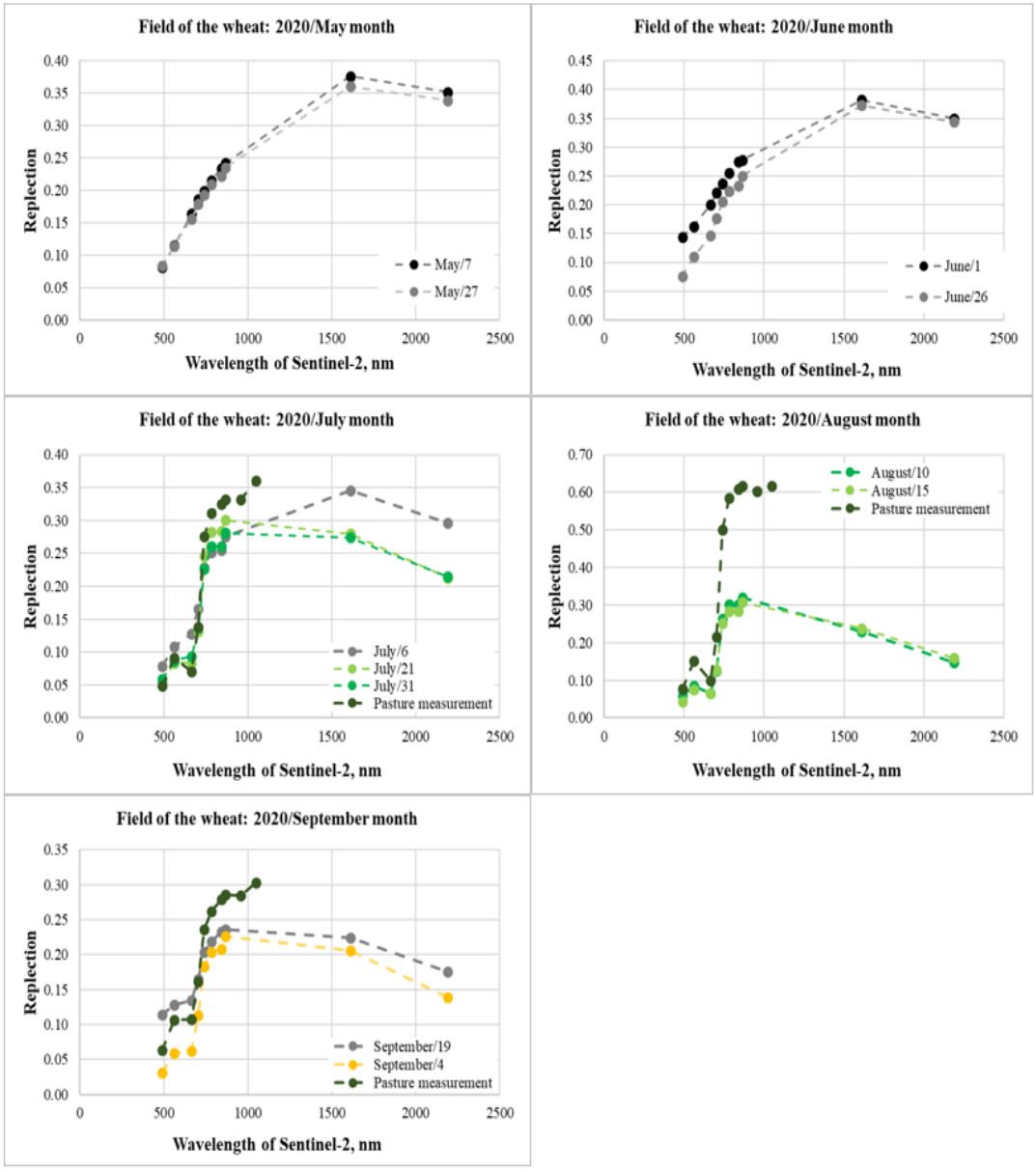

Fig. 8. Sentinel-2 Wavelength Reflection of Wheat Field (2020 May-September)

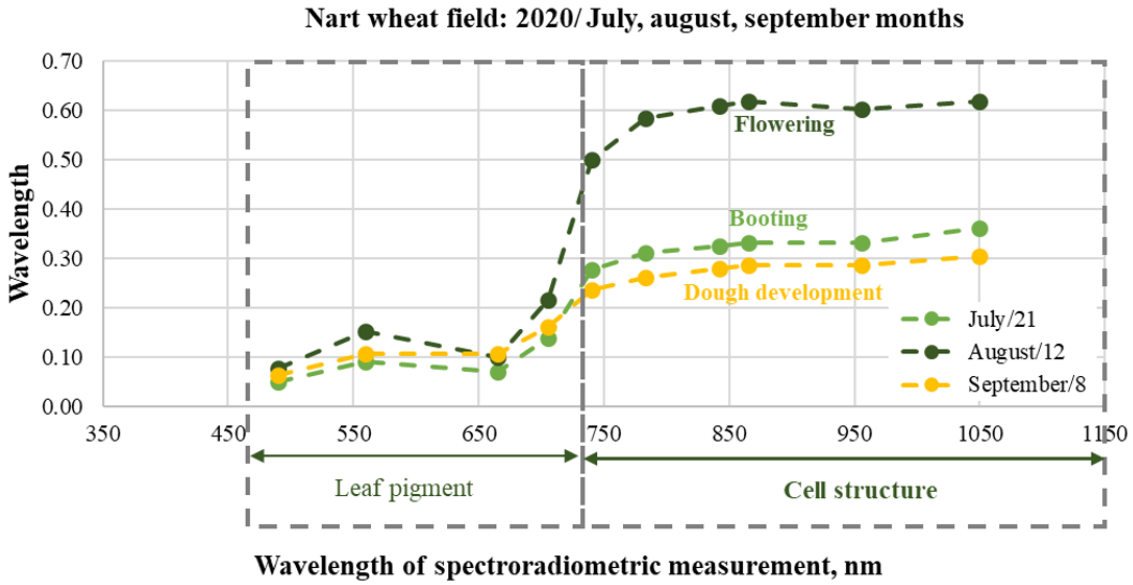

Fig. 9. Spectroradiometric measurements of the Nart field in July, August and September

changes in leaf color as the plants mature. A noticeable decrease occurs in the dough development stage (orange line), indicating less chlorophyll or pigment activity. Cell Structure (Green to Yellow range): Wavelengths associated with cell structure fluctuate during booting and head emergence (green and gray lines), reflecting the development of the plant's structural features. Water Content and Leaf Biochemistry (Blue range): The graph shows fluctuations in wavelengths that relate to water content and leaf biochemistry. These changes are most prominent during the flowering and dough development stages, indicating changes in the plant's hydration and biochemical composition. This graph highlights how Sentinel-2 wavelengths can effectively track changes in the wheat plants' physiological properties throughout their growing stages, from flowering to dough development.

This figure shows the Sentinel-2 wavelength reflection of wheat fields from May to September 2020 (Fig. 8). The x-axis represents the Sentinel-2 wavelengths (350-2500 nm), and the y-axis shows the reflection values. May: The reflection is low early in the month, increasing towards the end, indicating early growth. June: Reflection rises significantly, showing more vegetative growth and increased chlorophyll. July: Reflection increases further, peaking at the end of the month as the plants mature. August: The reflection is highest, indicating full vegetative and reproductive growth. September: Reflection starts to decrease, reflecting the plant's transition to maturity. These changes in reflection correspond to the wheat's growth stages from early development to full maturity.

In the Nart field, spectroradiometric measurements were conducted to monitor wheat reflectance across key phenological stages (Fig. 9). The results indicate that reflectance increased from early development to flowering and booting stages, peaking in August, before declining during the dough stage in September. These changes correspond to variations in leaf pigments (450-750 nm) and cell structure (750-1150 nm), highlighting stage-specific spectral signatures.

DISCUSSION

The growth and development of spring wheat in Bornuur soum, Mongolia, exhibited a highly structured phenological pattern, with distinct stages aligning closely with environmental conditions during the 2020 growing season. Observations every five days on selected plant samples confirmed the uniformity of vegetative stages, beginning with germination in early June and progressing through pod formation, flowering, and milk maturity by mid-September. These observations align with established agricultural calendars in temperate regions of Mongolia, indicating consistency in regional cultivation timelines.

Satellite-based analysis using Sentinel-2 imagery further supported these ground-based observations. NDVI values showed a significant increase from 0.18 in early May to a peak of 0.80 in July and September, reflecting the progressive canopy development and chlorophyll content in the wheat crop. The NDVI values demonstrated strong correlations with both wet biomass (R^2=0.67) and dry biomass (R=0.62), reinforcing the effectiveness of remote sensing vegetation indices in monitoring wheat phenology.

Additionally, NDWI proved useful in capturing soil and plant water conditions, a critical factor for wheat, which is highly sensitive to waterlogging. This sensitivity highlights the need for careful moisture monitoring, particularly under changing climatic conditions. Spectral reflectance values derived from Sentinel-2 ranged between 0.05-0.45 nm, with higher values observed in late-stage growth. Field spectroradiometric measurements further corroborated these patterns, showing a peak reflectance of 0.60 nm during flowering and a decline to 0.30 nm during the panicle stage. These reflectance shifts indicate specific phenophases and stress responses that remote sensing can reliably capture.

Together, these findings underscore the potential of integrating high-resolution remote sensing with phenological observation to improve monitoring and yield forecasting. They also provide actionable insights for policymakers and farmers in Mongolia facing climatic variability and resource constraints. Continued research should explore combining satellite data with predictive models to inform water management and pest control strategies, thereby enhancing wheat resilience in the face of climate change.

CONCLUSIONS

This study demonstrates the potential of integrating high-resolution Sentinel imagery with vegetation indices, such as NDVI and NDWI, to estimate wheat yield at the field scale. The results reveal a strong correlation between vegetation water indices and crop development metrics, providing valuable insights into the spatial-temporal dynamics of wheat growth. These findings emphasize the importance of advanced monitoring tools for local agricultural decision-making, particularly in Mongolia, where climate change exacerbates challenges to crop production and food security (Trivellone et al., 2022; Islam et al., 2024).

As global warming accelerates, Mongolia's agricultural sector is increasingly threatened by water stress, unpredictable weather patterns, and heightened risks of crop diseases (Brooks et al., 2019). This transition from sustainability to survival necessitates urgent, science-driven action plans to safeguard food security and crop resilience. Effective strategies should integrate remote sensing technologies, adaptive agricultural practices, and robust disease risk management systems to mitigate these threats. By addressing the interplay between food security and emerging infectious diseases, this approach aligns with the Stockholm Paradigm and Darwinian principles of proactive adaptation to environmental change (Brooks and Agosta, 2024a).

By bridging advanced remote sensing techniques with actionable policies, this study contributes to the development of a resilient agricultural framework, ensuring that wheat - a cornerstone crop for Mongolia - can thrive amid escalating environmental challenges. Future research should explore integrating these methods with predictive disease modeling and collaborative risk management to bolster agricultural sustainability in the Anthropocene (Brooks and Agosta, 2024b).

ACKNOWLEDGMENTS

This research was supported by the commissioned project of the Ministry of Food and Agriculture (Shu Uz 2019/02), through the Mongolian Foundation for Science and Technology, with funding provided by the Ministry of Education and Science.

REFERENCES

Brooks, D., Agosta, S. 2024b. Surviving the Anthropocene: A Darwinian Guide. Global Perspectives, vol. 5(1), 115331. https://doi.org/10.1525/gp.2024.115331

Brooks, D.R., Agosta, S.J. 2024a. A Darwinian Survival Guide: Hope for the Twenty-First Century. Cambridge, MA: MIT Press. https://doi.org/10.7551/mitpress/15069.001.0001

Brooks, D.R., Hoberg, E.P., Boeger, W.A. 2019. The Stockholm paradigm: Climate change and emerging disease. Chicago, USA: University of Chicago Press, 400 p.

Gansukh, B., Batsaikhan, B., Dorjsuren, A., Jamsran, C., Batsaikhan, N. 2020. Monitoring wheat crop growth parameters using time series Sentinel-1 and Sentinel-2 data for agricultural application in Mongolia. The International Archives of the Photogrammetry, Remote Sensing and Spatial Information Sciences, vol. XLIII-B3-2020, 989-994. https://doi.org/10.5194/isprs-archives-XLIII-B3-2020-989-2020

Gao, B.C. 1996. NDWI-A normalized difference water index for remote sensing of vegetation liquid water from space. Remote Sensing of Environment, vol. 58(3), p. 257-266. https://doi.org/10.1016/S0034-4257(96)00067-3

Ibrahim, G.R.F., Rasul, A., Abdullah, H. 2023. Improving crop classification accuracy with integrated Sentinel-1 and Sentinel-2 data: A case study of barley and wheat. Journal of Geovisualization and Spatial Analysis, vol. 7, 22. https://doi.org/10.1007/s41651-023-00152-2

IPCC. 2021. Climate Change 2021: The Physical Science Basis. IPCC Sixth Assessment Report, The Physical Science Basis. Cambridge University Press. https://www.ipcc.ch/report/ar6/wg1/

Islam, A.T., Islam, A.K.M.S., Islam, G.M.T., Bala, S.K., Salehin, M., Choudhury, A.K., Mahboob, M.G., Dey, N.C., Hossain, A. 2024. Monitoring wheat area using Sentinel-2 imagery and in-situ spectroradiometer data in heterogeneous field conditions. Discover Agriculture, vol. 2, 52. https://doi.org/10.1007/s44279-024-00069-4

Kornhuber, K., Osprey, S., Coumou, D., Petri, S., Petoukhov, V., Rahmstorf, S., Gray, L. 2019. Extreme weather events in early summer 2018 connected by a recurrent hemispheric wave-7 pattern. Environmental Research Letters, vol. 14(5), 054002. https://doi.org/10.1088/1748-9326/ab13bf

Yuping, M., Shili, W., Li, Z, Yingyu, H., Liwei, Z., Yanbo, H., Futang, W. 2008. Monitoring winter wheat growth in North China by combining a crop model and remote sensing data. International Journal of Applied Earth Observation and Geoinformation, 10(4), p. 426-437. https://doi.org/10.1016/j.jag.2007.09.002

Nduku, L., Munghemezulu, C., Mashaba-Munghemezulu, Z., Ratshiedana, P.E., Sibanda, S., Chirima, J.G. 2024. Synergetic Use of Sentinel-1 and Sentinel-2 Data for Wheat-Crop Height Monitoring Using Machine Learning. AgriEngineering, 6(2), p. 1093-1116. https://doi.org/10.3390/agriengineering6020063

Segarra, J., Araus, J.L., Kefauver, S.C. 2022. Farming and Earth observation: Sentinel-2 data to estimate within-field wheat grain yield. International Journal of Applied Earth Observation and Geoinformation, vol. 107, 102697. https://doi.org/10.1016/j.jag.2022.102697

Shao, Y., Lunetta, R.S., Wheeler, B., Iiames, J S., Campbell, J. B. 2016. An evaluation of time-series smoothing algorithms for land-cover classifications using MODIS-NDVI multitemporal data. Remote Sensing of Environment, vol. 174, p. 258-265. https://doi.org/10.1016/j.rse.2015.12.023

Shewry, P.R. 2009. Wheat. Journal of Experimental Botany, vol. 60(6), p. 1537-1553. https://doi.org/10.1093/jxb/erp058

Shojaeezadeh, S.A., Elnashar, A., Weber, T. K. D. 2025. A novel fusion of Sentinel-1 and Sentinel-2 with climate data for crop phenology estimation using Machine Learning. Science of Remote Sensing, vol. 11, 100227. https://doi.org/10.1016/j.srs.2025.100227

Toth, C., Jóźków, G. 2016. Remote sensing platforms and sensors: A survey. ISPRS Journal of Photogrammetry and Remote Sensing, vol. 115, p. 22-36. https://doi.org/10.1016/j.isprsjprs.2015.10.004

Trivellone, V., Hoberg, E.P., Boeger, W.A., Brooks, D.R. 2022. Food security and emerging infectious disease: Risk assessment and risk management. Royal Society Open Science, 211687. https://doi.org/10.1098/rsos.211687

Tuvdendorj, B., Wu, B., Zeng, H., Batdelger, G., Nanzad, L. 2019. Determination of appropriate remote sensing indices for spring

wheat yield estimation in Mongolia. Remote Sensing, vol. 11(21), 2568. https://doi.org/10.3390/rs11212568

Tuvshinbayar, D., Erdenetuya, B., Erkhembayar, E., Batbileg, B., Sarangerel, J. 2018. Some results of crop stress monitoring by remote sensing in Northern Mongolia. Mongolian Journal of Agricultural Sciences, vol. 21(02), p. 59-63. https://doi.org/10.5564/mjas.v21i02.906

Zhao, Y., Potgieter, A.B., Zhang, M., Wu, B., Hammer, G.L. 2020. Predicting wheat yield at the field scale by combining high-resolution Sentinel-2 satellite imagery and crop modelling. Remote Sensing, vol. 12(6), 1024. https://doi.org/10.3390/rs12061024